Modelled and Resolved Turbulent Stresses around a circular cylinder using URANS, DES and DDES

Naveed Durrani
Centres of Excellence in Science and Applied Technologies (CESAT), Islamabad, Pakistan

Abstract

Numerical flow analysis at Reynolds number 1.4×10^5 and 8.0×10^6 over a circular cylinder is carried out in this work. The comparison of the pressure coefficient over the surface of circular cylinder is carried out with the experimental data for these Reynolds numbers. Comparisons of computed Reynolds stresses are carried out with experimental data for DES and DDES. For massively separated flows, the resolved stresses have much bigger contribution than modelled stresses. A comparison of the modelled and resolved stresses is made at the $Re= 8\times10^6$ to appreciate their contribution. It is pointed that the contribution from both modelled and resolved Reynolds stresses give a better overall view of the Reynolds stresses of the flow. .

Key words

Massively separated flows, Detached Eddy Simulation (DES), Delayed Detached Eddy Simulation (DDES), Turbulence, Modelled Reynolds Stresses, Resolved Reynolds Stresses

Introduction

Numerical simulation of high Reynolds number turbulent flow over a circular cylinder is a common bench marking case for massively separated flows. The strong span-wise flow effects along with generation of large scales of eddies in the separated region aft of the cylinder makes it a favourite case for hybrid RANS-LES methodology such as DES[1] and DDES[2]. A circular cylinder of aspect ratio $\frac{L}{D}=2$ is taken for the present simulations consistent with study[3]. The Cp comparison of all the CFD simulations is carried out with the experimental work by Roshko[5] and Von Nunnen[6], in line with the other studies[3,4]. The experimental results by Cantwell [7] are used for the Reynolds stress comparison. The available data for each study is listed in the table 1. It is to be pointed out that due to this unavailability of complete set of experimental data, some of the simulation results at a particular Reynolds number are compared with different experimental Reynolds numbers, as done in other studies.

Experiment	Reynolds Number	Cp	Cf	Cd	Reynolds Stresses
Roshko[5]	$8.5\text{x}10^6$	√	X	√	X
Cantwell [7]	$1.4\text{x}10^5$	** (Large variations in data)	X	1.237	√
Von Nunnen[6]	$7.6\text{x}10^6$	√	X	√	X

Table 1 *Details of different available experimental data for circular cylinder*

Numerical Scheme:

Detached eddy simulation (DES)

The Detached Eddy Simulation approach (DES) was proposed by Spalart et al. in 1997[1]. The original DES proposed combines the RANS and LES in a non-zonal manner. DES is based on the Spalart-Allmaras one equation turbulence model [8]. Length scale, d, is generally taken as the shortest distance at any point to the closest wall in RANS mode. In DES, it is replaced with the minimum between the distance to the wall and a length proportional to the local grid spacing. It is represented mathematically as

$$d_{\mathrm{DES}} = \min(d, C_{\mathrm{DES}}\,\Delta) \tag{1}$$

where, C_{DES} represents a model constant taken as 0.65 in different studies[1]. Δ is the local grid spacing. For structured grids, it is the maximum grid spacing over all three directions. For unstructured grids, it is generally taken as the maximum edge length connecting the centroids of the adjacent cells.

Delayed Detached eddy simulation (DDES)

The main idea of DDES is to include the molecular and turbulent viscosity information into the switching mechanism to delay this switching in boundary layers.

$$\tilde{d} \equiv d - f_d \max(0, \mathrm{d\text{-}C}_{DES}\,\Delta) \tag{2}$$

$$f_d \equiv \tanh\left(\left[8 r_d\right]^3\right) \tag{3}$$

$$r_d \equiv \frac{\nu_t + \nu}{\sqrt{U_{i,j}U_{i,j}}\,\kappa^2 d^2} \tag{4}$$

The details of this modification are presented in Ref [2].

Governing equations

$$\frac{\partial}{\partial t}\iiint_V \underbrace{\mathbf{W}}_{\text{Conservative variables}} dV + \iint_{\partial A}\left[\underbrace{\mathbf{F}}_{\text{inviscid flux}} - \underbrace{\mathbf{G}}_{\text{viscous flux}}\right].d\mathbf{A} = 0 \tag{5}$$

where primitive variable matrix Q is presented as,

$$\mathbf{Q} = \begin{pmatrix} p \\ u \\ v \\ w \\ T \end{pmatrix} \text{ and } \mathbf{W} = \begin{Bmatrix} \rho \\ \rho u \\ \rho v \\ \rho w \\ \rho E \end{Bmatrix}, \qquad \mathbf{F} = \begin{pmatrix} \mathbf{F}_x \\ \mathbf{F}_y \\ \mathbf{F}_z \end{pmatrix}, \ \mathbf{G} = \begin{pmatrix} \mathbf{G}_x \\ \mathbf{G}_y \\ \mathbf{G}_z \end{pmatrix}$$

$$\mathbf{F}_x = \begin{Bmatrix} \rho u \\ \rho uu + p \\ \rho uv \\ \rho uw \\ \rho uE + pu \end{Bmatrix}, \qquad \mathbf{G}_x = \begin{Bmatrix} 0 \\ \tau_{xx} \\ \tau_{xy} \\ \tau_{xz} \\ u\tau_{xx} + v\tau_{xy} + w\tau_{xz} - q_x \end{Bmatrix}$$

$$\mathbf{F}_y = \begin{Bmatrix} \rho v \\ \rho vu \\ \rho vv + p \\ \rho vw \\ \rho vE + pv \end{Bmatrix}, \qquad \mathbf{G}_y = \begin{Bmatrix} 0 \\ \tau_{yx} \\ \tau_{yy} \\ \tau_{yz} \\ u\tau_{yx} + v\tau_{yy} + w\tau_{yz} - q_y \end{Bmatrix}$$

$$\mathbf{F}_z = \begin{Bmatrix} \rho w \\ \rho wu \\ \rho wv \\ \rho ww + p \\ \rho wE + pw \end{Bmatrix}, \qquad \mathbf{G}_z = \begin{Bmatrix} 0 \\ \tau_{zx} \\ \tau_{zy} \\ \tau_{zz} \\ u\tau_{zx} + v\tau_{zy} + w\tau_{zz} - q_z \end{Bmatrix}$$

Dual-time stepping:

$$\underbrace{\frac{\partial}{\partial t}\iiint_V \mathbf{W}dV}_{Physical\,time\,term} + \underbrace{\mathbf{\Gamma}\frac{\partial}{\partial \tau}\iiint_V \mathbf{Q}dV}_{Pseudo\,time\,term} = -\mathbf{K}^{-1}\mathbf{K} * \iint_A [\mathbf{F} - \mathbf{G}].d\mathbf{A} \tag{6}$$

Reynolds Number $1.4x10^5$

Mesh Statistics

Table 2 presents the mesh statistics with different cell types used in the mesh.

Number of nodes	Number of elements	Type of cells		
		Brick	Tetrahedral	Pyramid
405259	1789623	110880	1675047	3696

Table 2 *Mesh statistics of circular cylinder with L/D=2 for $Re=1.4\times10^5$*

Domain at the inlet and outlet is 35 times the radius of the cylinder and on top and bottom sides is 20 times the radius of the cylinder. All the meshes are generated using commercial software Gambit[9].

Numerical simulation details

Table 3 presents the numerical simulation details and different parameters used for the CFD simulation.

Reynolds Number	Mach Number	Velocity (m/sec)	Inviscid Flux Scheme	Turbulence Scheme
$1.4x10^5$	0.288	100	Roe	DES/DDES

Table 3 *Case details of simulation*

Mesh details with the surface mesh and element distribution in the near-wall and wake region are shown in figure 1.

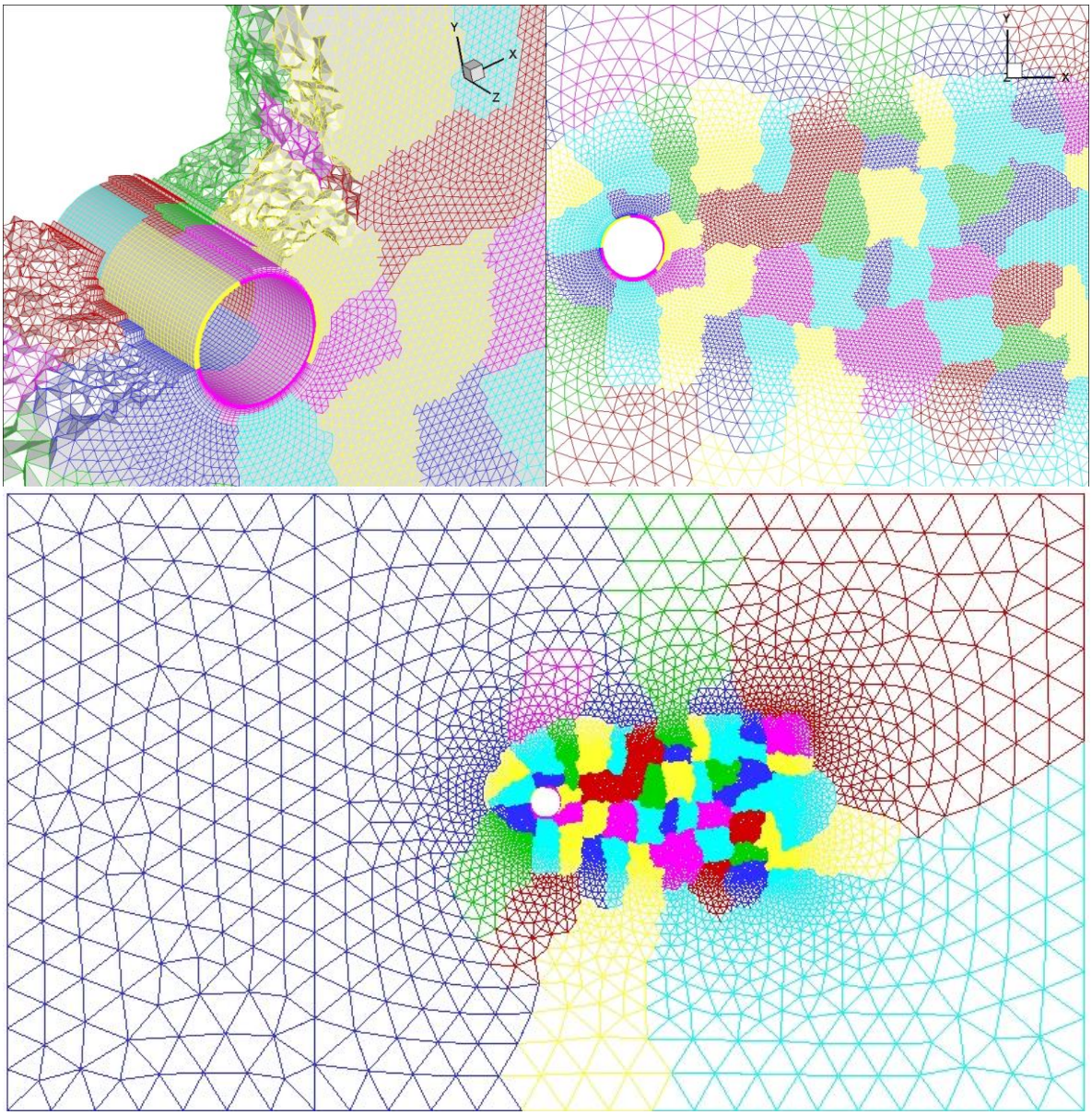

Figure 1 Grid Details with parallel partitions

Fig. 2 indicates that the Y+ value over the whole cylinder surface does not exceed 0.3.

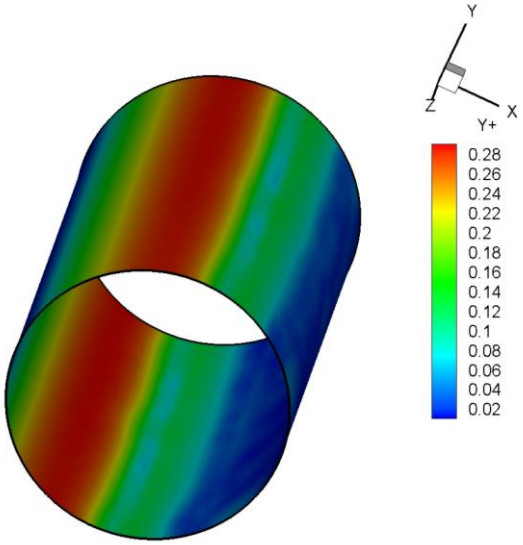

Figure 2 *Y+ values over the surface of circular cylinder at Re=1.4×10^5*

It was observed during simulations that the S-A model is quite sensitive to first cell height. For very low Y+ value, the convergence achieved is very good and for Y+ values over 1, the turbulence equations do not converge well. The strong dependence of S-A model on first cell height is consistent with similar observations from other studies [10]. There are 44 cells along the span-wise direction on the cylinder surface resulting in $\frac{\Delta_Z}{D} \approx 0.0455$.

Results

In order to obtain the correct statistics for Strouhal number and or shedding frequency, it is recommended to start with a very short physical time step for the flow simulation. The results obtained indicate the scale of temporal variations. Subsequently, the physical time step can be increased to obtain better temporal efficiency for physical time.

The 2nd order spatial accuracy is obtained with the piecewise linear reconstruction of the flow variables. The higher spatial accuracy presents better flow field results. The comparison of the lift and drag coefficients using both DES and DDES hybrid RANS-LES schemes is presented against time (seconds) in figure 3. An important observation is that for this case which is termed as 'natural DES' case, the results from DDES closely follow the DES results.

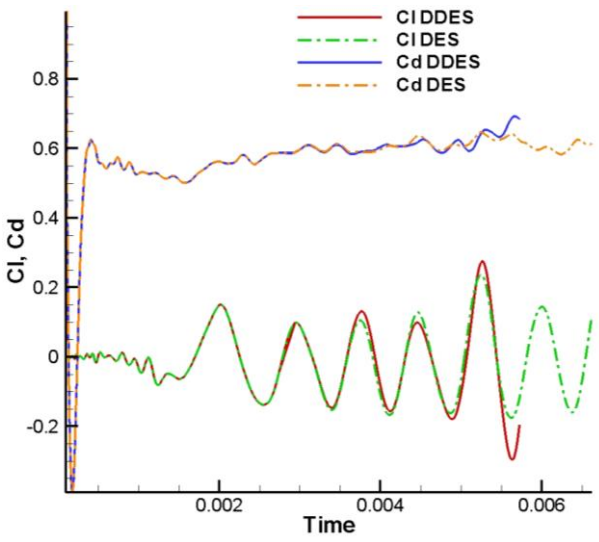

Figure 3 *Comparison of time averaged C_l and C_d values computed by DGDES using DES and DDES. Time step is very small, 5×10^{-7} seconds with data showing around 12000 iterations data. X-axis represents physical time in seconds.*

One shedding cycle is about 1600 iterations as plotted in figure 3. Idea of starting from a very small time step is to obtain the correct Strouhal number statistics. Based on this, the time step can be increased with confidence that the time accuracy will be sufficient to present correct time dependant phenomenon provided that the bigger time step gives the same strouhal number. The DDES and DES solutions start to differ in terms of shedding cycle and associated lift and drag values. In the next simulation, the time step is increased to $5x10^{-5}$ for subsequent simulations. The data input (length of data on plot figure) of DDES is shorter than DES in figure 3 and 4. It is intentionally put in this way to appreciate the extra cost associated with DDES. Both simulations were run for the same amount of time using same number of processors and compilation flags. The extra computational cost associate with the DDES scheme is due to the calculation of the switching parameter for each iteration.

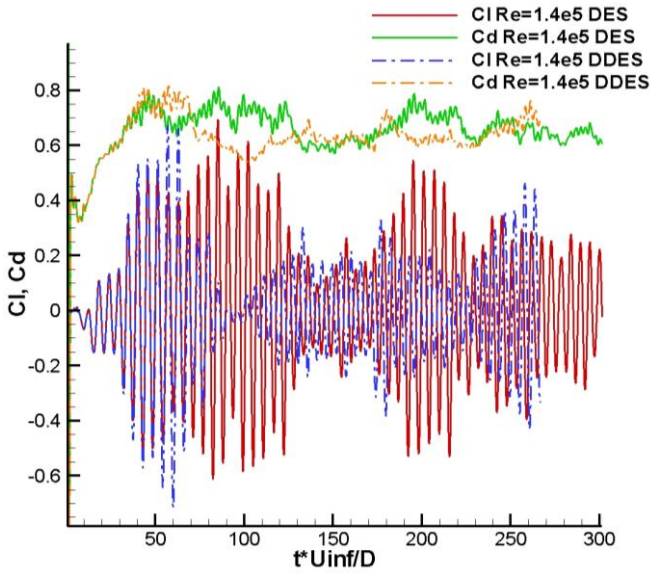

Figure 4 *Comparison of time averaged C_l and C_d values computed by DGDES using DES and DDES. Time step is 5×10^{-5}*

The comparison of this study with the other studies and experimental data at a different Reynolds number of $3.6x10^6$ is presented in figure 7. The experimental Cp data for this Reynolds number has a large variation as described in table 1, thus it is compared with higher Reynolds number experimental data of $3.6x10^6$, similar to other studies[3,4].

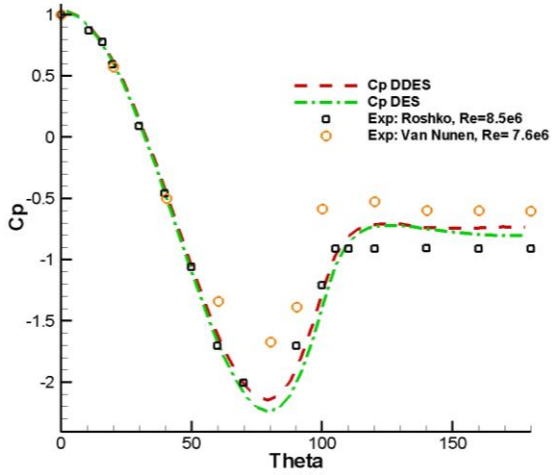

Figure 5 *Comparison of Cp values computed by DGDES using DES and DDES with experimental data at $Re=1.4\times10^5$*

The Cp plot from the DES simulation indicates a deeper –Cp region in comparison with the DDES simulation, as presented in figure 5. The available experimental data results for comparison, which are at higher Reynolds number than these simulations, indicates a similar trend. 'Exp' in figure 5 indicates the experimental data.

Probe data extraction for DES and DDES flow field analysis

A subroutine was added in DG-DES which can read in the probe locations from an input file and then locate these probes in individual partitions of the mesh and subsequently extract the data to a separate output file for each probe.

A probe point located at the centre line with 2 diameters downstream of the cylinder. The recorded data is analysed for the comparison of the DES and DDES output. Fig 6 indicates the power spectral density plot of recorded data using the DES and DDES scheme. It is evident that energy cascade as discussed in

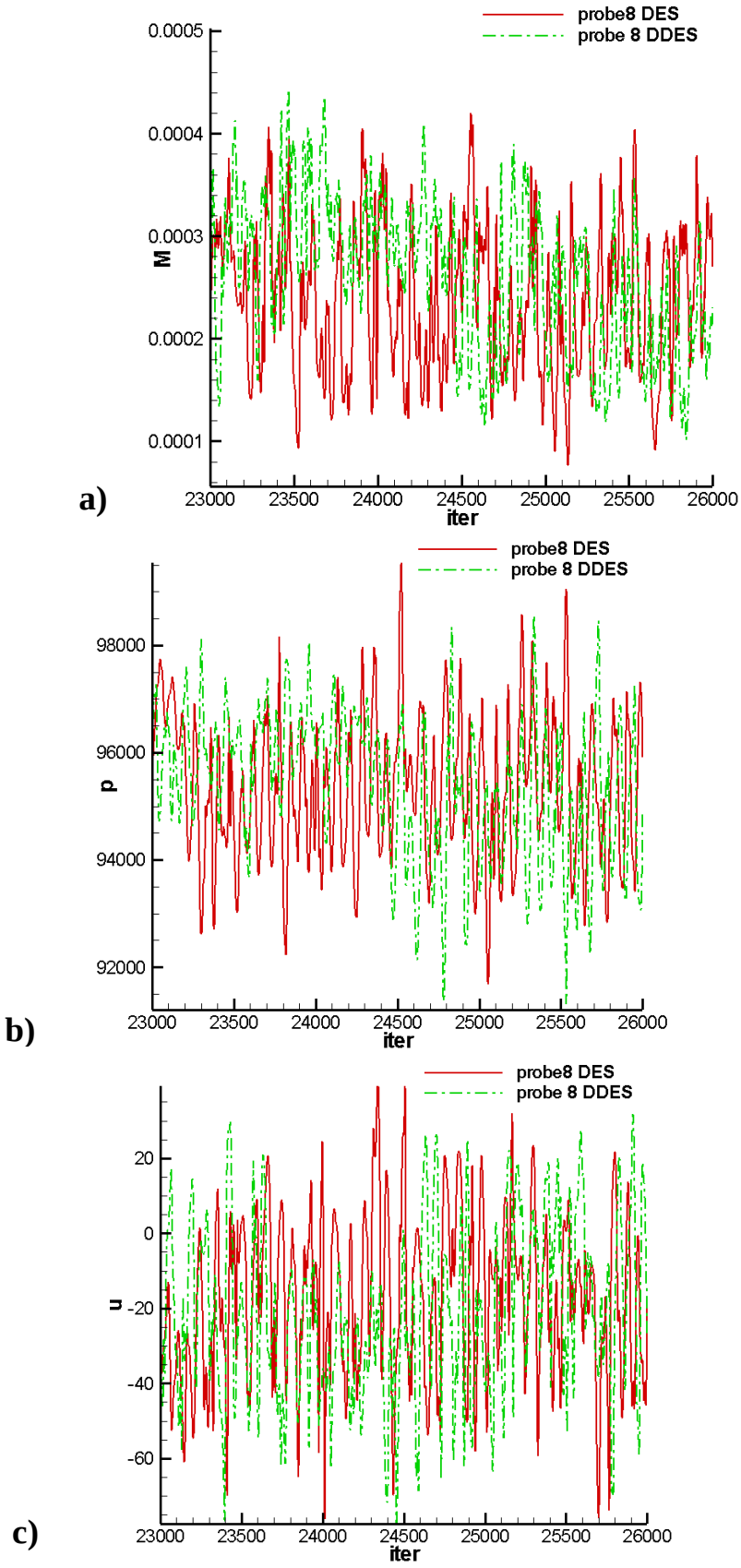

Figure 6(a-c) *Recorded data at different iterations probe using the DES and DDES schemes*
a)Turbulent viscosity b) static pressure c) x-direction velocity

The other observation from the probes data is that the completely different flowfield variable values at the probe location with varying time are obtained, as presented in figure 6(a-c).

Summary of the results Re=1.4x10^5

Table 3 presents the overall comparison of results at Re=1.4x10^5. It is clear that the results are quite encouraging. C_{pb} or base pressure is more negative in comparison with other studies. It may be improved by using finer mesh as used in Ref.[4]. Generally the results are satisfactory.

Case	**Cd**	**St**	**_C_{pb}**	θ_{sep}
DG-DES DES97	0.66	0.29	0.80	101°
DG-DES DDES	0.64	0.29	0.77	100°
Travin et al.[3]	0.65	0.28	0.70	93°
DES 97 Krishnan et al.[4]	0.58	0.29	0.64	98°
DDES Krishnan et al.[4]	0.60	0.28	0.69	99°
Roshko[5]	0.62-0.74	0.27	----	----

Table 4 *Summary of results Re=1.4×10^5*

Comparison of the velocity flow field in the domain

Travin et. al (Ref. [3]) present the comparison of time averaged normalized velocity field in the domain with the experimental data as a measure of quality of the solution. Fig 7 is the comparison with the upper half as simulation and the lower half as the experimental data.

The overall comparison is encouraging and the present simulation is in better agreement with the experimental data given in it.

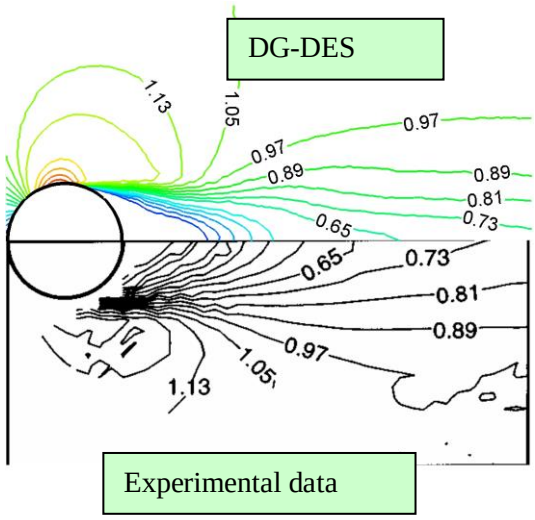

Figure 7 *Upper side DG-DES simulation lower side experimental data*

Derivation of the Modelled Reynolds Stress formula (based on Bradshaw's Formulation[11])

In 1877, Boussinesq provided a solution for turbulence closure. This approximation assumes that the principal axes of the Reynolds stress tensor are coincident with the mean strain-rate tensor throughout the domain on all points. He assumed that the turbulence stresses are directly proportional to the velocity gradient with eddy viscosity (μ_t) as the constant of proportionality and only unknown value. This value further can be calculated using different turbulence models.

From Boussinesq hypothesis [12], the eddy viscosity is linearly related with Reynolds turbulent stresses. Although, the assumption of μ_t as an isotropic scalar quantity in the Boussinesq hypothesis may not be strictly true. Other option is to go for more computationally expensive Reynolds stress transport equations. S-A model used in this study utilizes the Boussinesq hypothesis.

The basic relationship is drawn from analogy with molecular transport of momentum

$$\overline{u_i' u_j'} = \frac{2}{3}(k)\delta_{ij} - \nu_t\left(\frac{\partial U_i}{\partial x_j} + \frac{\partial U_j}{\partial x_i}\right)$$

It provides the following normal ad shear stress components for Reynolds stresses:

$$\overline{u'u'} = \frac{2}{3}(k) - \nu_t\left(\frac{\partial U}{\partial x} + \frac{\partial U}{\partial x}\right)$$

$$\overline{v'v'} = \frac{2}{3}(k) - \nu_t\left(\frac{\partial V}{\partial y} + \frac{\partial V}{\partial y}\right)$$

$$\overline{u'v'} = -\nu_t\left(\frac{\partial U}{\partial y} + \frac{\partial V}{\partial x}\right)$$

Where U and V are the mean velocity components. For two-equation turbulence models using turbulent kinetic energy (k) as a variable in the equation, k is calculated from solution of those equations. However, in one equation S-A turbulence model, k is not explicitly calculated. Hence, it is to be approximated using Bradshaw's hypothesis [11].

The turbulent energy equation for a two-dimensional incompressible mean flow, outside the viscous sublayer, is (Townsend 1956)[13]

$$q^2 = u'^2 + v'^2 + w'^2 = 2k$$

$$\tau = -\rho\overline{u'v'}$$

$$\underbrace{\frac{1}{2}\rho\left(U\frac{\overline{\partial q^2}}{\partial x} + V\frac{\overline{\partial q^2}}{\partial y}\right)}_{\text{advection}} - \underbrace{\tau\frac{\partial U}{\partial y}}_{\text{Production}} + \underbrace{\frac{\partial}{\partial y}\left(\overline{pv} + \frac{1}{2}\rho\overline{q^2 v}\right)}_{\text{diffusion}} + \underbrace{\rho\varepsilon}_{\text{dissipation}} = 0$$

And $\varepsilon \simeq \upsilon \overline{\left(\frac{\partial u_i}{\partial x_j} \right)^2}$

It can be regarded as an equation for the advection or rate of change of turbulent kinetic energy along a mean streamline through a point if all the other terms as known at that point, just as the boundary-layer momentum equation,

$$\rho \left[U \frac{\partial U}{\partial x} + V \frac{\partial U}{\partial y} \right] = \rho U_1 \frac{dU_1}{dx} + \frac{\partial \tau}{\partial y}$$

It can be regarded as an equation for the rate of change of mean-flow momentum ρU .

By defining:

$$a1 \equiv \frac{\tau}{\rho \overline{q^2}},\ L \equiv \frac{\left(\frac{\tau}{\rho} \right)^{\frac{3}{2}}}{\varepsilon}$$

$$G \equiv \frac{\left(\frac{\overline{pv}}{\rho} + \frac{1}{2} \overline{q^2 v} \right)}{\left(\frac{\tau_{\max}}{\rho} \right)^{\frac{1}{2}} \frac{\tau}{\rho}}$$

The choice of empirical functions (Page 599, Ref. [13]):

$$a1 \equiv \frac{\tau}{\rho \overline{q^2}} = 0.15$$

$$a1 = \frac{-\rho \overline{uv}}{\rho \left(\overline{u'^2} + \overline{v'^2} + \overline{w'^2} \right)}$$

$$a1 = \frac{\tau}{\frac{1}{2} \rho \overline{q^2}} = 0.3$$

$$a1 = \frac{\tau}{k} = 0.3$$

Considering a 2D log law boundary layer, put $a1 = \sqrt{C_\mu}$ $(\Rightarrow C_\mu = 0.09)$

$$\frac{\tau}{k} = \sqrt{C_\mu}$$

$$k = \frac{\tau}{\sqrt{C_\mu}} \qquad \therefore \tau = -\rho \overline{uv}$$

Putting back values:

$$k = \frac{\nu_t \left| \frac{\partial u}{\partial y} \right|}{\sqrt{C_\mu}} = \frac{\nu_t S^*}{\sqrt{C_\mu}} \qquad \therefore \quad S^* = \sqrt{2 S_{ij} S_{ij}}$$

$$S_{ij} = \frac{1}{2}\left(\frac{\partial U_i}{\partial x_j} + \frac{\partial U_j}{\partial x_i} \right)$$

Resolved Turbulent Reynolds Stresses

Resolved stresses are computed in the code after establishing that the solution is mature (after sufficient shedding cycles, the vortex shedding establishes a more regularized pattern). A parameter, 'rssavfr' representing Reynolds stresses saving frequency, is defined in the initialization file to describe the number of iterations after which the data is accumulated for calculation of the Reynolds stresses. Two other recording parameters tr1 and tr2 are specified in the initialization file which corresponds to the start and end time of this data recording. It is imperative to make sure that this time is sufficient enough for recording of the Reynolds stresses. In all the simulations, at least 20 shedding cycles are taken for recording of the Reynolds stresses and the values are sampled at each iteration. The symbol $\langle \ \rangle$ represents the variable averaged values over the specified number of iterations.

$$\overline{u'u'} = \langle uu \rangle - \langle u \rangle^2$$
$$\overline{v'v'} = \langle vv \rangle - \langle v \rangle^2$$
$$\overline{u'v'} = \langle uv \rangle - \langle u \rangle \langle v \rangle$$

Comparison of the Reynolds stresses from the DES simulation with the experimental data [7]

For any turbulent flow simulation, the comparison of the Reynolds stresses is very important but equally challenging. This comparison provides an overall resemblance of the real time flow turbulence compared with the simulation. The favourable comparison will indicate that the flow being simulated results in a good representation of the actual experimental or real life flowfield. However, if the Reynolds stresses are not correct, even if the aerodynamic coefficients are the in good agreement with the experimental data, the accuracy of the simulation will be doubtful. However, this is a particular aspect that may prove difficult to match due to the different factors. These factors include the scheme efficiency, mesh type and quality and the numerical dissipation in the solver. The Reynolds stresses have not been presented frequently in the previous studies.

Experimental data

DG-DES

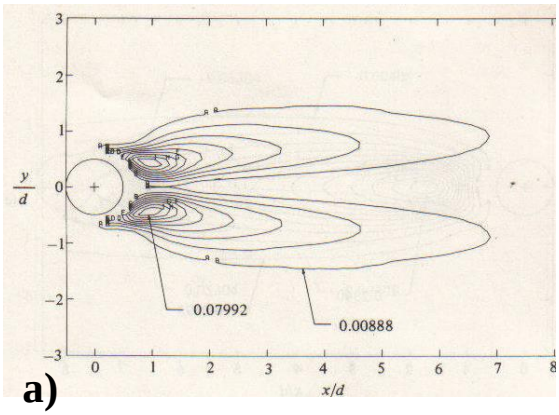

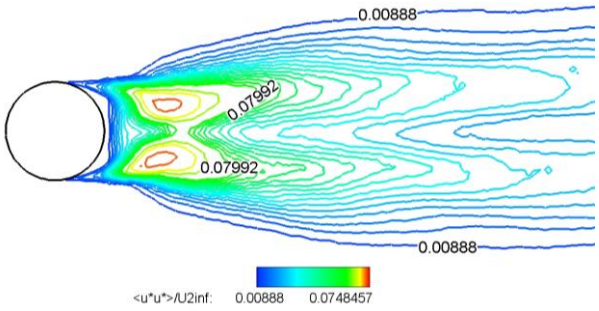

a)

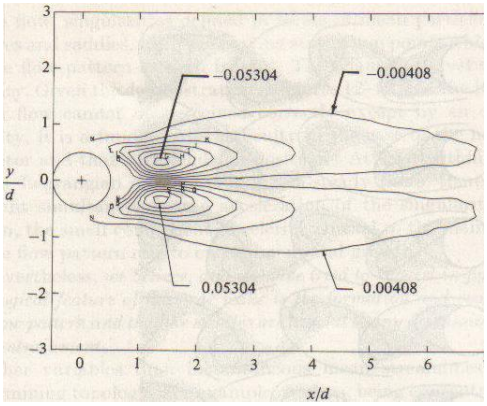

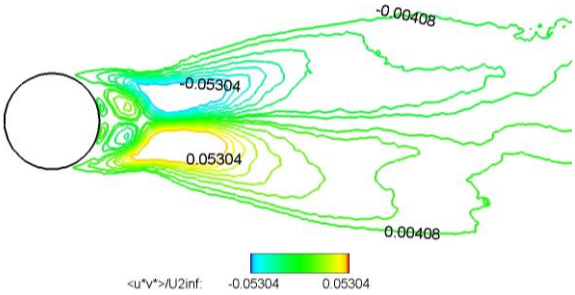

b)

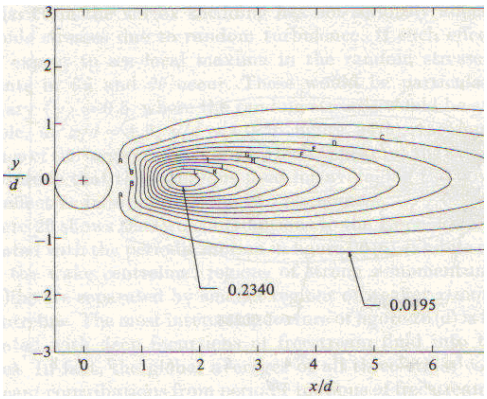

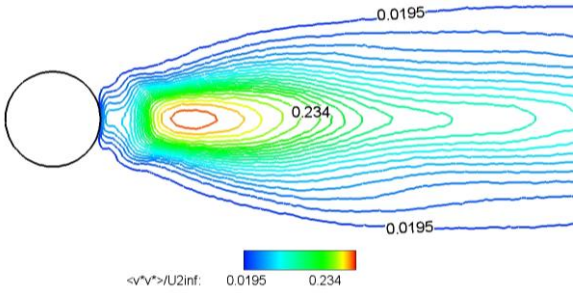

c)

Figure 8 *Comparison of the experimental Reynolds stresses [7] at Re=1.4×10^5 with the DES simulation at Re=1.4×10^5*

a) $< u^* u^* > / U_{\text{inf}}^2$ *left: Experimental right: DES simulation*

b) $< u^* v^* > / U_{\text{inf}}^2$ *left: Experimental right: DES simulation*

c) $< v^* v^* > / U_{\text{inf}}^2$ *left: Experimental right: DES simulation*

The general comparison, as presented in figure 8, is encouraging. The structure of the Reynolds stresses obtained from the DES solution is quite similar to the experimental data. Although, the respective levels are not at same locations, but keeping in view the nature of simulation and size of the mesh being used, it is quite satisfactory. Keeping in view the assumptions in the CFD simulations and the different

uncertainties in the experiment, the overall quality of the results is quite reasonable. It is quite challenging to get good match of the simulated results with the experimental data.

Circular cylinder at Reynolds number 8x10^6

Yplus (Y+)

Similar to previous simulations, the Y+ value of less than 1 is sought.

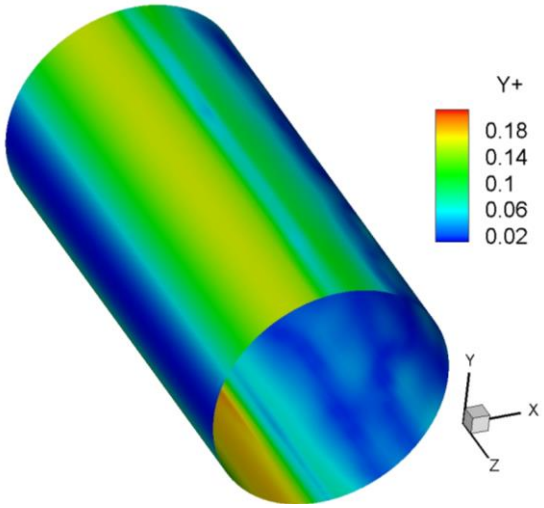

Figure 9 *Y+ values over the surface of circular cylinder at Re=8×10^6*

Y+ value of well below 1 is obtained as presented in figure 9.

C_l C_d plot circular cylinder at Reynolds number 8x10^6

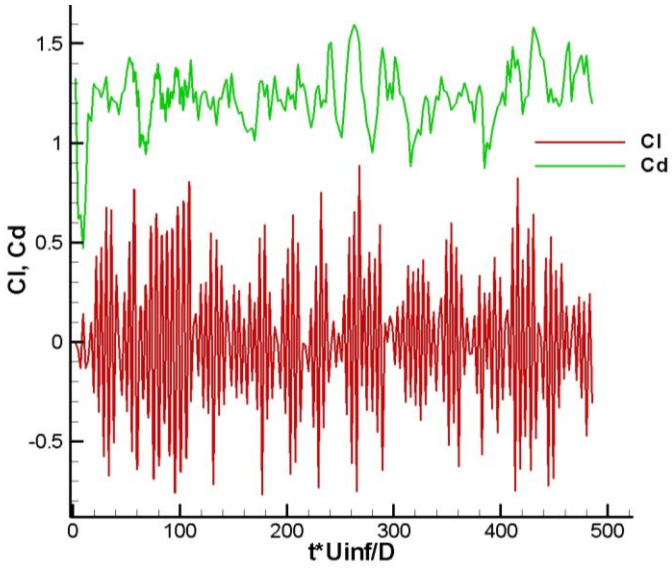

Figure 10 *C_l and C_d of circular cylinder at Re=8×10^6 using the DES scheme*

Due to a large number of length scales of the vortices being shed from the circular cylinder, the lift and drag have varying amplitudes of modulations in their time history as presented in figure 10. It is typical of a massively separated flow field exerting fluctuating forces on the body of disturbance (object).

Vorticity magnitude contours

The short physical time step of $1x10^{-5}$ sec clearly indicates more detail and more length scales in the flow in comparison with time step of $5x10^{-5}$ (fig. 11 and fig. 12). It can be argued that certain small length scales are captured by short time step that results in the form generation of extra details which are skipped or dissipated by the large time step. Also, the solution is not expected to be very similar due to the LES dominated solver application in the flow.

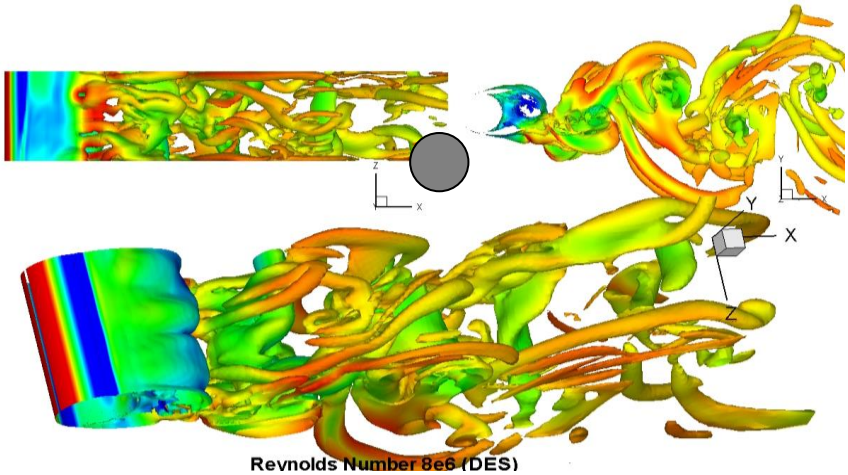

Figure 11 *DES flow simulation of circular cylinder at Reynolds number = 8×10^6 at t=0.4575sec. Instanataneous iso-surface plot of vorticity magnitude 1000 coloured by static Pressure Top (left) : View from bottom side Top(right) View from side Bottom: Isometric View*

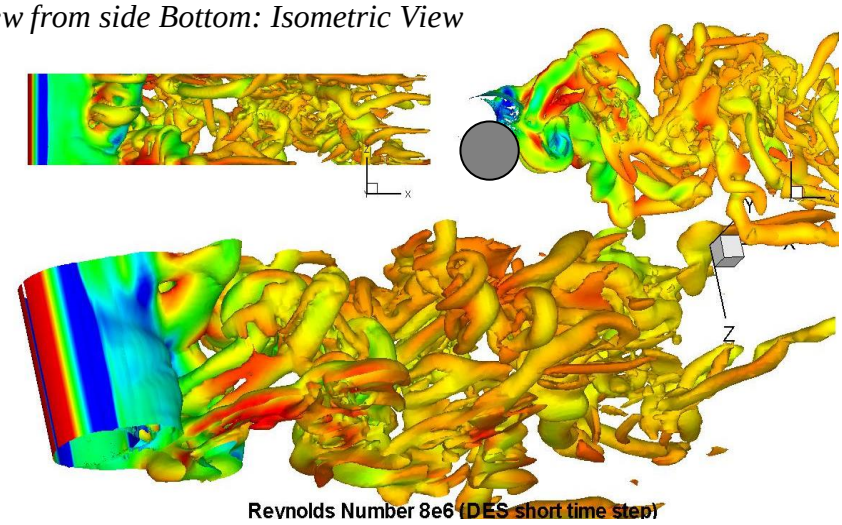

Figure 12 *DES flow simulation of circular cylinder at Reynolds number 8 $\times10^6$. Instantaneous iso-surface plot of vorticity magnitude 1000 at t=0.4575sec., coloured by static Pressure*
Top (left) : View from bottom side Top(right) View from side Bottom: Isometric View

Comparison of modelled and resolved stresses using the DES scheme

For highly separated flows, it is important to compute both modelled and resolved stresses. Although, resolved stresses have a dominant role, the modelled stresses may have significant contribution as well. Generally the modelled Reynolds stresses are more dominant in boundary and shear layers with relatively insignificant contribution from resolved stresses for attached flows. However,

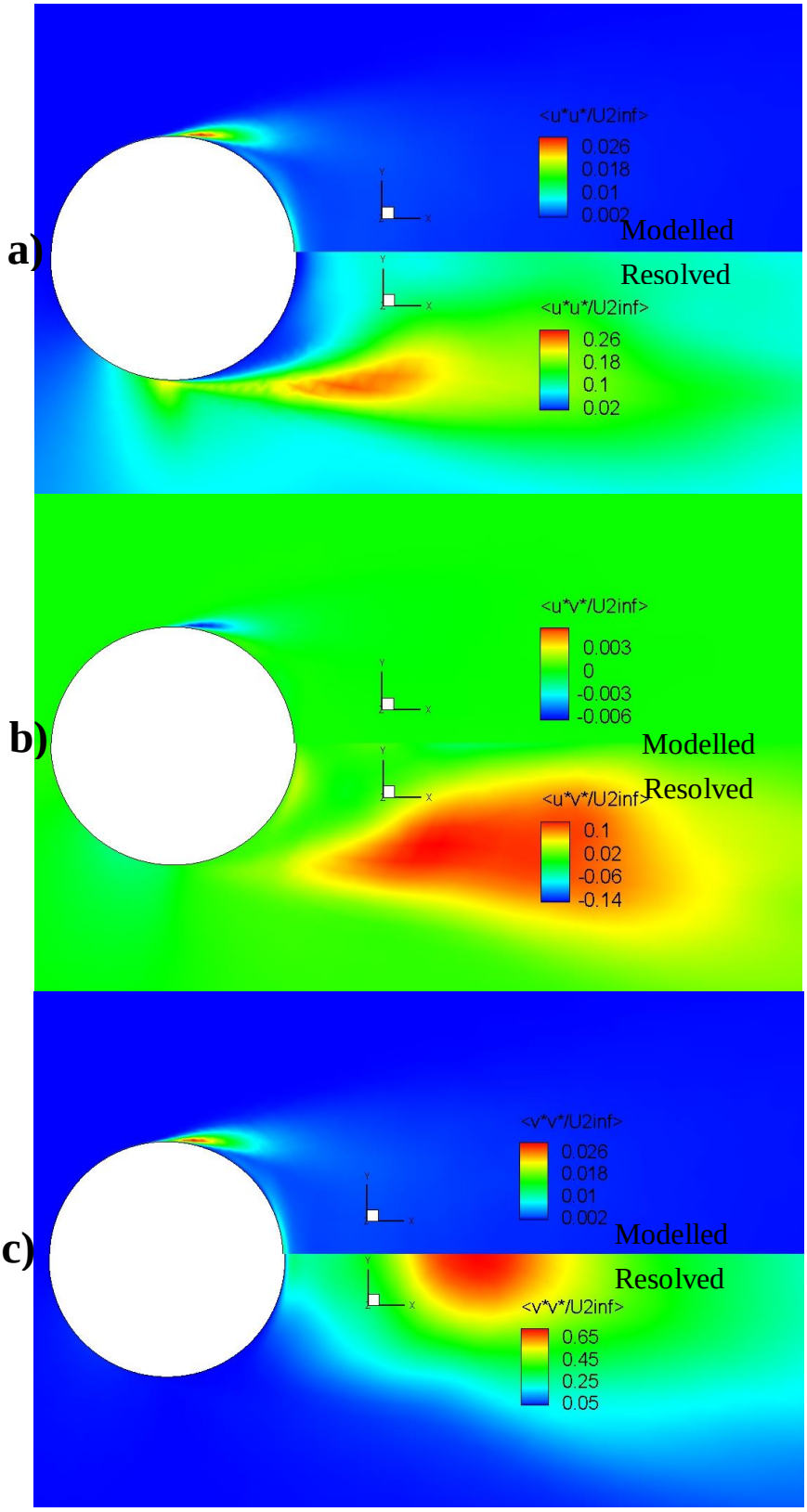

Figure 13 *Comparison of modelled and resolved stresses using DES simulation at Re=8×10^6*
Upper half is modelled stresses and lower half is resolved stresses.
a) $<u^*u^*>/U_{inf}^2$ *b)* $<u^*v^*>/U_{inf}^2$ *c)* $<v^*v^*>/U_{inf}^2$

for massively separated flowfields, the resolved stresses play a dominant role. In hybrid schemes like DES, it is important to appreciate the contribution by both modelled and resolved stresses. Generally for mild separation, it is better to present the Reynolds stresses as an accumulative contribution by both modelled and resolved stresses. Figure 13 presents a comparison of modelled and resolved stresses for Re=8x10^6. It is evident that the resolved stresses are clearly a dominant contributor of the overall Reynolds stresses. Roughly, $<u^*u^*>/U_{inf}^2$ contribution from resolved stresses is 10 times that from the modelled one. The $<u^*v^*>/U_{inf}^2$ contribution from resolved stress is 30 times that of the modelled stress and $<v^*v^*>/U_{inf}^2$ contribution from the resolved stress is 25 times that of the modelled stress. It indicates that although the contribution from the modelled stresses is roughly an order of magnitude lower than the resolved stresses for this case yet the modelled stresses cannot be neglected. One point to notice is the concentration location of these stresses. The resolved stresses near the surface of the circular cylinder (boundary layer and shear layer region etc.) are negligible; however, these are the areas of maximum stress contribution by modelled stresses.

Hence, to obtain an overall close proximity of the Reynolds stresses, these stresses should be added in the domain.

Conclusions

The high Reynolds number flows over circular cylinder are natural DES cases. The blunt body with high Reynolds number flows causes the massive separation and instability in the downstream direction of circular cylinder in the domain. The new turbulent viscosity generated by this phenomenon is independent of the upstream turbulent viscosity.

The three commonly reported cases for high Reynolds number flows over circular cylinder are simulated at Reynolds number of 1.4x10^5 and 8.0x10^6. The overall results are very encouraging and the flowfield turbulence, vortical structures and flow parameters are well captured. The shedding frequency, pressure distribution and skin friction coefficient values of the simulated results match well with the other published studies. The computed resolved stresses also provide satisfactory comparison with the experimental data, better than one of the reported studies which is done with coarser than present grid. This particularly is very encouraging from the perspective of the applicability of the hybrid RANS-LES methodology for massively separated flow at Reynolds numbers which are still prohibited by LES simulations. The size of the grid used is roughly an order less than what is generally required by LES simulations.

References

1. Spalart, P. R., Jou W-H., Strelets M., Allmaras, S. R., "Comments on the Feasibility of LES for Wings and on a Hybrid RANS/LES Approach" Advances in DNS/LES, 1st AFOSR Int. Conf. on DNS/LES, Greyden Press, Columbus Oh, 4-8 August, 1997.
2. Spalart, P., Deck, S., Shur, M., Squires, K., Strelets, M. K., and Travin, A., "A New Version of Detached-Eddy Simulation, Resistant to Ambiguous Grid Densities," Theoretical and Computational Fluid Dynamics. 0935-4964, pp.181-195, July 2006.
3. A. Travin, M. Shur, M. Strelets and P. Spalart, "Detached-Eddy Simulation past a Circular Cylinder", Journal of Flow, Turbulence and Combustion, 63, 269-291, 1999.
4. Krishnan, V. and Squires, K. D., Forsythe, J. R., "Prediction of Flow Around a Circular Cylinder at High Reynolds Number", AIAA 2006-901, 44th AIAA Aerospace Sciences Meeting and Exhibit, Reno, Nevada, 9-12 January 2006.
5. Roshko, A., "Experiments on the Flow past a Circular Cylinder at Very High Reynolds Number", Journal of Fluid Mechanics, Vol. 10, No. 3, pp. 345-356, 1961.
6. Nunen, J. V., "Pressure and Forces on a Circular Cylinder in a Cross flow at High Reynolds Numbers", Flow Induced Structural Vibrations, Springer-Verlag, Berlin, pp. 748-754, 1974.
7. Cantwell, B. and Coles, D., "An experimental study of entrainment and transport in the turbulent near wake of a circular cylinder." Journal of Fluid Mechanics, Vol. 136, pp. 321- 374, Nov. 1983.
8. P. R. Spalart and S. R. Allmaras, "A One-Equation Turbulence Model for Aerodynamic Flows", AIAA Paper 92-0439, January 1992.
9. http://www.fluent.com/software/gambit.
10. Cokljat, D. and Liu, F., "DES of turbulent flow over an airfoil at high incidence ," AIAA paper 2002-0590, at 40th Aerospace Sciences Meeting and Exhibit, 14-17 January 2002, Reno Nevada., 2002.
11. P. Bradshaw, D. H. Ferriss and N. P. Atwell, "Calculation of boundary-layer development using the turbulent energy equation", Journal of Fluid Mechanics, 28:3:593-616, Cambridge University Press. Aerodynamics Division, National Physical Laboratory, Teddington, 1967.
12. J. O. Hinze. "Turbulence ", McGraw-Hill, New York, 1975.
13. Townsend, A. A., The Structure of Turbulent Shear Flow. Cambridge University Press.1956.